

Modelling epidemic dynamics under collective decision making

Mengbin Ye^{1,*}, Lorenzo Zino^{2,*}, Alessandro Rizzo^{3,4,†} & Ming Cao^{2,†}

¹*Optus–Curtin Centre of Excellence in Artificial Intelligence, Curtin University, Perth, Australia*

²*Faculty of Science and Engineering, University of Groningen, Groningen, Netherlands*

³*Dipartimento di Elettronica e Telecomunicazioni, Politecnico di Torino, Torino, Italy*

⁴*Office of Innovation, New York University Tandon School of Engineering, Brooklyn NY, USA*

During the course of an epidemic, individuals constantly make decisions on how to fight against epidemic spreading^{1–5}. Collectively, these individual decisions are critical to the global outcome of the epidemic, especially when no pharmaceutical interventions are available^{6–8}.

However, existing epidemic models lack the ability to capture this complex decision-making process, which is shaped by an interplay of factors including government-mandated policy interventions, expected socio-economic costs, perceived infection risks and social influences. Here, we introduce a novel parsimonious model, grounded in evolutionary game theory, able to capture decision-making dynamics over heterogeneous time scales⁹. Using real data, we analyse three case studies in the spreading of gonorrhoea, the 1918–19 Spanish flu and COVID-19. Behavioural factors shaping the course of the epidemic are intelligibly mapped onto a minimal set of model parameters, and their interplay gives rise to characteristic phenomena, such as sustained periodic outbreaks, multiple epidemic waves, or a

*These authors contributed equally.

†These authors contributed equally.

successful eradication of the disease. Our model enables a direct assessment of the epidemiological and socio-economic impact of different policy interventions implemented to combat epidemic outbreaks. Besides the common-sense finding that stringent non-pharmaceutical interventions are essential to taming the initial phases of the outbreak, the duration of such interventions and the way they are phased out are key for an eradication in the medium-to-long term. Surprisingly, our findings reveal that social influence is a double-edged sword in the control of epidemics, helping strengthen collective adoption of self-protective behaviours during the early stages of the epidemic, but then accelerating their rejection upon lifting of non-pharmaceutical containment interventions.

1 Introduction

In the absence of pharmaceutical interventions, slowing or eradicating an epidemic in a population crucially depends on the actions of a sufficiently large number of individuals to adopt appropriate behavioural responses such as physical distancing or wearing face masks. However, such human behaviours are typically not considered in classical mathematical epidemic models¹⁰, including those for the ongoing COVID-19 pandemic^{11–13}. To bridge this gap, recent efforts have led to individual behavioural responses being incorporated into mathematical epidemic models^{1–4}. However, even these recent works suffer from a simplistic focus on the concept of individual awareness: while it is true that the awareness of an outbreak drives individuals to adopt self-protective behaviours to reduce the probability of becoming infected^{14,15}, recent lessons on the complexity of human behaviours from the COVID-19 outbreak have exposed inherent limitations of awareness-

based modelling mechanisms⁵. In particular, such mechanisms are often purely instantaneous and reactive, thus failing to capture the very factors that affect time-varying behavioural responses over the whole duration of an epidemic, such as social influence and perceived socio-economic costs. An additional salient aspect highlighted by COVID-19 is the impact of government-mandated policy interventions on individuals' decision-making processes^{7,8,16}. Finally, high levels of uncertainty cause bounded rationality to become prominent in an individual's decision making, which is seldom included in current behavioural-epidemic models¹⁷.

Here, we move the focus from the instantaneous impact of reactive and fully rational behavioural responses at the onset of an epidemic (as in awareness-based models) to a long-term outlook where complex behavioural dynamics arise for each individual. To this end, our model is based on an evolutionary game approach that is able to capture bounded rational decision-making processes that evolve over the long term⁹. Our approach enables the explicit inclusion of the most salient factors that each individual balances and trades off when deciding their behavioural response to an epidemic outbreak, such as social influence, perceived infection risks, policy interventions by authorities and the accumulation of socio-economic costs¹⁸. This allows for a better assessment of the effectiveness of different policy interventions from a healthcare point of view, while also evaluating their socio-economic impacts^{19,20}.

We demonstrate our paradigm by incorporating it into two exemplary epidemic progression models and applying them to three real-world case studies, including an instance of periodic outbreaks of gonorrhoea and the 1918 Spanish flu pandemic, for which it consistently reproduces the

historical occurrence of consecutive waves of infections. We also shed light on several “what-if” scenarios of relevance to the current COVID-19 outbreak, covering the whole course of the epidemic evolution. Notably, we show that in the early stages, weak interventions can lead to a general failure to adopt self-protective behaviours, resulting in multiple overlapping infection waves. On the other hand, we demonstrate that in the advanced phases of the epidemic evolution, the time over which a phased reduction of a lockdown occurs, rather than the severity of the initial lockdown itself, determines whether a second infectious wave appears, yielding severe health and socio-economic consequences. Importantly, we identify that social influence acts as a double-edged sword, providing benefits during the early stages of a lockdown, but accelerating the collective rejection of self-protective behaviours during its phased reduction.

2 Model

We consider a population $\mathcal{V} = \{1, \dots, n\}$ of n individuals. Each individual $i \in \mathcal{V}$ is characterised by a two-dimensional variable $(x_i(t), y_i(t))$, which models their *health state* and the *social behaviour* adopted at the discrete time $t \in \mathbb{Z}_{\geq 0}$, respectively.

The variable $x_i(t) \in \mathcal{A}$ takes values in a discrete set of health states \mathcal{A} . For the sake of simplicity, we start by introducing our paradigm in combination with the well-known susceptible–infected–susceptible (SIS) epidemic model²¹, which is characterised by two health states: S represents *susceptible* individuals, who are healthy and can be infected by the disease upon interacting with *infected* individuals, represented by the state I . A global observable $z(t)$ measures the *de-*

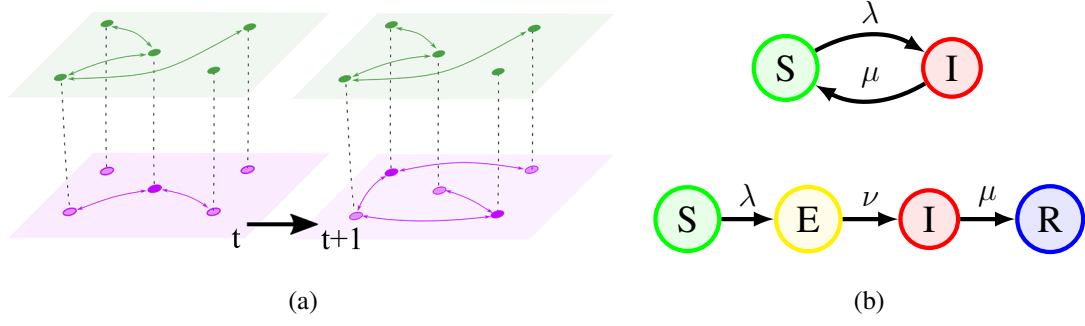


Figure 1: Illustration of the network model and the epidemic progression. In (a), two time-steps in the two-layer network representation. The upper layer (green) shows influences, the lower layer (violet) contacts. In (b), schematics of the state transitions of the SIS model (above) and of the SEIR model (below). The constants λ , μ and ν indicate transition probabilities.

tectable prevalence of the epidemic disease at time t : $z(t) = \frac{1}{n} |\{i : x_i(t) = I\}|$, where $|\cdot|$ denotes a set's cardinality. Further health states may be added to the set \mathcal{A} to capture specific features of the disease being studied²¹.

The social behaviour of individual i is captured by the binary variable $y_i(t) \in \{0, 1\}$ that expresses whether the individual adopts self-protective behaviours ($y_i(t) = 1$) or continues as normal ($y_i(t) = 0$). The paradigm is amenable to extensions to capture different levels of self-protection through modification of the support set of $y_i(t)$.

The spread of the disease and the individuals' decision-making processes co-evolve, mutually influencing one another on a two-layered network structure $\mathcal{G} = (\mathcal{V}, \mathcal{E}_I, \mathcal{E}_C(t))$, illustrated in Fig. 1a. The set of undirected links \mathcal{E}_I defines the static *influence layer*, capturing *social influence* between individuals during the decision-making process. The *contact layer* is defined through a

time-varying set of undirected links $\mathcal{E}_C(t)$, which represent the *physical contacts* between pairs of individuals that may result in the transmission of the disease. We model the contact layer using an activity-driven network (ADN)²², which captures important features of complexity that characterise real-world networks. In ADNs, a constant parameter $a_i \in [0, 1]$, called *activity*, expresses individual i 's propensity to generate $m \geq 1$ interactions with other individuals at each discrete time instant. Details are provided in the Methods.

Epidemic Spread At each discrete time-step t , every individual i that is susceptible and does not adopt self-protections (i.e. $x_i(t) = S$ and $y_i(t) = 0$) may become infected. A constant parameter $\lambda \in [0, 1]$, termed *infection probability*, captures the probability that the disease is transmitted by an infectious individual ($x_j(t) = I$) to a susceptible one through physical contact. We assume that an individual adopting self-protection, $y_i(t) = 1$, is always successful in preventing contagion. Beside the contagion, at each time-step t , every infected individual i recovers with probability $\mu \in (0, 1]$, becoming susceptible again to the disease. These transitions are illustrated in Fig. 1b, while technical details are provided in the Methods.

Human Behaviour Concurrently with the epidemic evolution, at each time-step t , each individual enacts a decision-making process on the adoption of self-protective behaviours, according to an evolutionary game-based mechanism termed logit learning⁹. The resulting behaviour is updated in a probabilistic fashion. We define two *payoff* functions $\pi_i(0)$ and $\pi_i(1)$, which represent a combination of socio-psychological, economic and personal benefits received by individual i for enacting behaviours $y_i = 0$ and $y_i = 1$, respectively. This individual then adopts self-protective

behaviours with a probability equal to

$$\mathbb{P}[y_i(t+1) = 1] = \frac{\exp\{\beta\pi_i(1)\}}{\exp\{\beta\pi_i(0)\} + \exp\{\beta\pi_i(1)\}}. \quad (1)$$

The parameter $\beta \in [0, \infty)$ measures an individual's *rationality* in the decision-making process; the larger the parameter β , the higher the probability that the individual chooses the behaviour that maximises their payoff. Payoffs are defined as

$$\pi_i(0) := \frac{1}{d_i} \sum_{j:(i,j) \in \mathcal{E}_I} (1 - y_j(t)) - u(t), \quad (2a)$$

$$\pi_i(1) := \frac{1}{d_i} \sum_{j:(i,j) \in \mathcal{E}_I} y_j(t) + r(z(t)) - f_i(t), \quad (2b)$$

and contain the following four terms, directly related to behavioural and social factors that shape the epidemic dynamics (more details can be found in the Methods).

- **Social influence.** The first summation terms in Eqs. (2a) and (2b) are inherited from coordination games on networks²³. These terms capture the *social influence* of neighbouring individuals and the individual's desire to coordinate with them, as it provides an increased payoff for adopting the same behaviour as that adopted by the majority of the neighbours.
- **Policy interventions.** The time-varying term $u(t) \geq 0$ in Eq. (2a) captures a broad range of *non-pharmaceutical interventions* enforced by public authorities to discourage dangerous behaviours, e.g. by means of a fine or imprisonment or by providing benefits for working from home.
- **Risk perception.** The *risk-perception function* $r(z) : [0, 1] \rightarrow \mathbb{R}_{\geq 0}$ in Eq. (2b) is a monotonically non-decreasing function of the detectable prevalence z , which captures an incentive to

adopt self-protective behaviour due to the endogenous fear of becoming infected as the disease spreads. Individuals may learn of z from the media coverage of the epidemic evolution. For simplicity, here we assume that all individuals share the same risk-perception function.

- **Cost of self-protective behaviour.** The negative impact of adopting self-protective behaviours is captured in Eq. (2b) by the *frustration function*

$$f_i(t) = c + \sum_{s=1}^t \gamma^s c y_i(t-s), \quad (3)$$

where $c \geq 0$ is the social, psychological and economic *immediate cost* per unit-time associated with the adoption of self-protective behaviours, e.g. related to the inability to socialise, work from the office, enjoy public spaces, etc., and $\gamma \in [0, 1]$ is its *accumulation factor*¹⁹. Thus, $f_i(t) \geq 0$ reflects accumulative costs for individual i up to time t .

Impact of an Epidemic Outbreak A major strength of the proposed paradigm lies in its ability to facilitate a thorough evaluation of the immediate health and socio-economic impact of an epidemic outbreak due to the population's behavioural responses to prescribed policy interventions, a task that has been considered extremely challenging so far^{18,20}. In fact, our formalism enables the direct computation of the *health cost*, which is directly related to the health state of individuals (i.e. $x_i(t)$), and the *socio-economic cost*, which depends on the behaviours adopted by the population (i.e. $y_i(t)$). By evaluating these costs for all individuals in the population, a cumulative health cost H (for example, the percentage of the population infected) and socio-economic cost C for the epidemic as a whole can be determined. More details and the explicit expression of these quantities used in the discussion of the case studies below can be found in the Methods.

3 Results

Onset of the Epidemic For large populations and fully connected influence layers, we use a mean-field approach²⁴ to obtain insight into the behaviour of the system at the initial stages of the epidemic through the computation of the epidemic threshold. In the absence of cumulative frustration (which is a reasonable assumption in the early stages of an outbreak) and assuming a constant intervention $u(t) = \bar{u}$, the outbreak is quickly eradicated if

$$\frac{\lambda}{\mu} < \frac{e^{\beta(1-\bar{u})} + (1-\beta)e^{-\beta c}}{m(\langle a \rangle + \sqrt{\langle a^2 \rangle})(e^{\beta(1-\bar{u})} - \beta e^{-\beta c})}, \quad (4)$$

where $\langle a \rangle$ and $\langle a^2 \rangle$ are the average and second moment of the activity distribution, respectively (the derivation of Eq. (4) can be found in the Methods). Figure 2 shows that mild non-pharmaceutical interventions (small \bar{u}) have only a minor impact on the epidemic threshold, since they may not provide a sufficient incentive to abandon the status-quo non-protective behaviours. On the other hand, the epidemic threshold increases significantly if \bar{u} is sufficiently large. The socio-economic cost c also plays an important role, whereby small increases can lower the threshold even for large \bar{u} . This implies that the perception of a high socio-economic cost may hamper the outcome of strong non-pharmaceutical interventions.

The threshold in Eq. (4) offers insight into the role of human behaviour in the early stages of an epidemic outbreak. We now move to the medium/long-term horizon, and consider scenarios in which the threshold is exceeded, yielding a large initial outbreak across the population. To shed light on the potential of our method, we present three case studies based on real data, viz. gonorrhoea, Spanish flu and COVID-19. To model the spread of gonorrhoea we use the basic SIS model

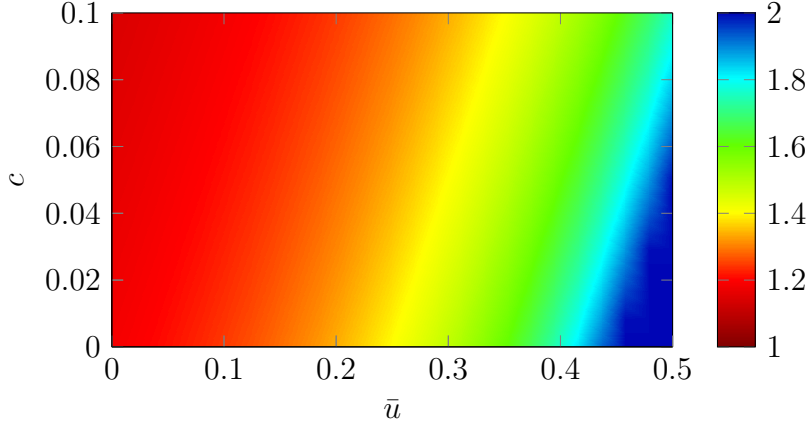


Figure 2: Ratio between the epidemic threshold computed in Eq. (4) and the corresponding quantity without self-protective behaviours²² as a function of the cost of adopting self-protective behaviours c and of policy interventions \bar{u} ($\beta = 2$). The larger this ratio (i.e. in the blue region), the more resistant the system is to the epidemic outbreak.

described earlier; to capture the latency period after contagion and immunity after recovery or death relevant to Spanish flu and COVID-19, we adopt a susceptible–exposed–infectious–removed (SEIR) model²¹, as described in the Methods and illustrated in Fig. 1b. Parameters are also detailed in the Methods.

SIS Modelling of Gonorrhoea Spreading Despite its simplicity, the SIS model has found an important application in the study of gonorrhoea outbreaks²⁵. We focus on revealing the role of the risk perception function $r(z)$ in shaping the epidemic outbreak and the behavioural response. Hence, we fix all other parameters and assume that no policy interventions are implemented. In Fig. 3, we consider three scenarios with progressively less cautious populations, showing that this shift in risk perception changes not only the quantitative, but also the qualitative, characteristic

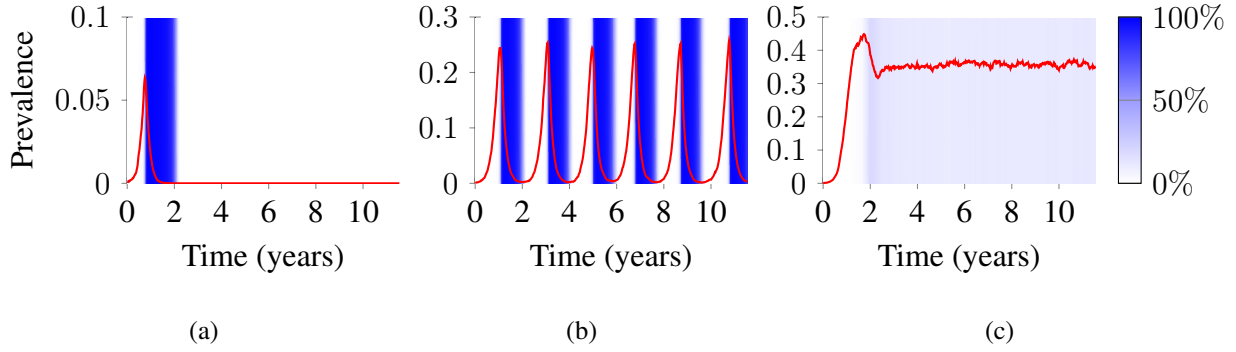


Figure 3: Prevalence of gonorrhoea infections (red curve) as a function of time as predicted by an SIS model using our co-evolution paradigm. The colour intensity of the blue vertical bands indicates the level of adoption of self-protective behaviours, i.e. $\frac{1}{n} \sum_{i=1}^n y_i$. In (a), a responsive population ($r(z) = 3\sqrt{z}$) results in quick adoption of self-protective behaviours and fast eradication of the disease, after the first wave. In (b), multiple waves emerge in a less cautious population ($r(z) = 3z$), yielding periodic waves of reinfection. In (c), in a population that underestimates the risk ($r(z) = 3z^2$), the disease becomes endemic and a meta-stable equilibrium emerges. Parameters are defined in the Methods.

phenomena observed. This demonstrates the power of our model, which allows to capture and reproduce a range of real-world phenomena within a unified modelling framework. In fact, by tuning just one parameter in the decision-making mechanism, we shift from fast eradication of the disease (Fig. 3a), to periodic oscillations both in the epidemic prevalence and in the behavioural response (Fig. 3b), and to the emergence of a meta-stable endemic equilibrium with a pervasive and long-term diffusion of the disease (Fig. 3c).

Notice that, as further detailed in the Methods, the risk perception function determines a

critical prevalence which guarantees a pervasive adoption of self-protections regardless of the behaviour of others. In our first scenario, this critical prevalence is $z^* \approx 18\%$. However, as can be observed in Fig. 3a, social influence causes individuals to rapidly and widely adopt self-protective behaviours much earlier, when the prevalence is $z(t) \approx 6\%$, highlighting the key role played by social influence in shaping collective behavioural patterns and, in this instance, helping in the fast eradication of the disease.

SEIR Modelling of the Spanish Flu Pandemic We use an SEIR model combined with our paradigm to reproduce the 1918–19 Spanish flu pandemic (see Methods). Using only model parameters rooted in the actual historical context, the simulation results in Figure 4 are qualitatively consistent with the epidemiological data that witnessed a resurgent pandemic with three waves including a massive second one^{6,26}. More importantly, key contributing factors identified from our model predictions as leading to the resurgence of new and even larger outbreaks also reflect historical observations. In particular, a slowly increasing risk perception — associated with the initial suppression of news about the flu²⁷ — results in a delay of over a month after the initial outbreak for the population to adopt self-protective behaviours. Meanwhile, a fast accumulating frustration (corresponding for example to the emergence of anti-mask movements at the time) results in self-protective behaviours being abandoned immediately when the epidemic prevalence decreases.

By doubling the duration of the interventions (from 28 days, as reported in the literature⁶, to 56 days) or by relying on a more responsive population (details in the Methods), only a single wave is witnessed, consistent with the historical fact that some cities successfully stopped the Spanish

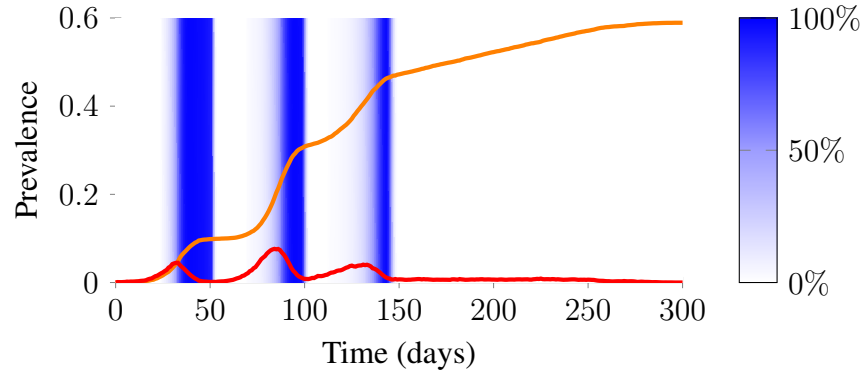


Figure 4: Prevalence of Spanish flu infections (red curve) and cumulative infections (orange curve) as a function of time as predicted by an SEIR model in combination with the co-evolution paradigm. The colour intensity of the blue vertical bands represents the fraction of adopters of self-protective behaviours. Our simulation qualitatively reproduces the 1918–19 pandemic outbreak with three consecutive epidemic waves. The impact of the outbreak is measured by health cost $H = 59.91\%$ and socio-economic cost $C = 6.02$, as detailed in the Methods.

flu through longer, timely interventions²⁸. The health costs in terms of cumulative epidemic prevalence is reduced from 59% to 11% and 4%, respectively, while the socio-economic costs associated with the adoption of self-protective behaviours are reduced by more than 50% (see Methods and Supplementary Fig. S1). This illustrates the power of our paradigm for predicting future scenarios once a particular parametrisation and model have been secured from empirical data. Existing approaches typically estimate how infection parameters, associated with the disease dynamics, are explicitly changed due to policy interventions¹¹. In contrast, our paradigm leaves the disease dynamics untouched, and allows policy interventions to influence the decision-making process, thus determining the behavioural responses, which, in turn, shape the epidemic evolution.

Modelling of the COVID-19 Pandemic Having established that our model reproduces key features of past epidemics, we now demonstrate its power as a predictive tool by analysing several different intervention scenarios for the ongoing COVID-19 pandemic¹³. To this end, we again integrate our game-theoretical framework into an SEIR model. In each of the simulations, we consider the same cost and accumulation factor, and a population that is slow to perceive COVID-19 as a threat; by varying the intervention strategies, and the level of social influence, we reveal the global impact of these factors.

Firstly, we observe that mild policy interventions, even if indefinite in duration, may not be sufficient to ensure a timely and collective adoption of self-protective behaviours. For instance, the population in Fig. 5a is overwhelmed by the epidemic because social influence acts as inertia to delay the adoption of self-protective behaviours (Supplementary Fig. S2)²⁹. Then, we consider two

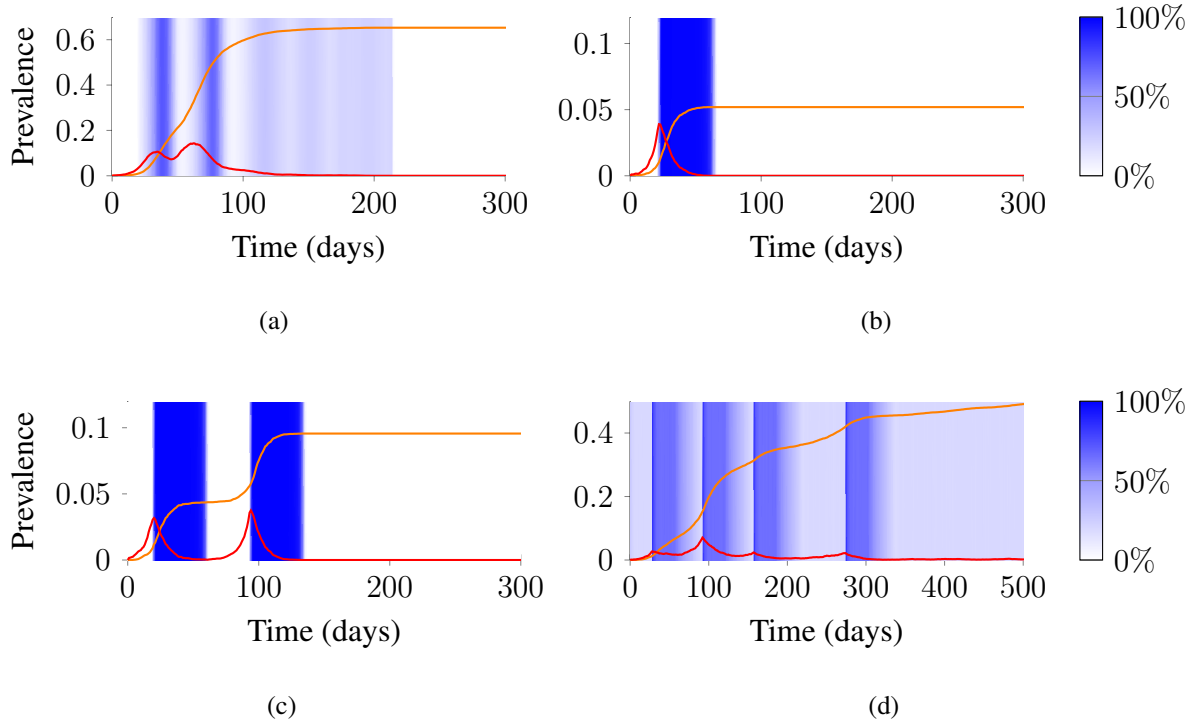


Figure 5: Prevalence of COVID-19 infections (red curve) and cumulative infections (orange curve) as a function of time as predicted by an SEIR model in combination with the co-evolution paradigm. The colour intensity of the blue vertical bands represents the fraction of adopters of self-protective behaviours. In (a), a mild policy intervention and accumulating frustration results in sporadic adoption of self-protection, and thus two massive epidemic waves that overlap and a long tail (health cost $H = 65.29\%$, socio-economic cost $C = 15.55$). In (b), a severe policy intervention with a long phased reduction period keeps the epidemic outbreak contained to a single wave ($H = 5.19\%$, $C = 12.24$). In (c), a very severe policy intervention with a short phased reduction period results in two consecutive epidemic waves ($H = 9.56\%$, $C = 23.79$). In (d), the policy in (b) is implemented in a scenario without social influence, showing that social influence is key to guaranteed collective (and thus effective) behavioural responses ($H = 49.58\%$, $C = 60.34$). Parameters and costs are detailed in the Methods.

scenarios with severe but short policy interventions, followed by a linear phased reduction (Figs. 5b and 5c; in the first scenario, the policy is less severe but the reduction period is longer). Comparing the two scenarios, we conclude that, provided that the initial policy interventions are sufficiently severe (to avoid the scenario shown in Fig. 5a), the successful eradication of the disease depends primarily on the phased reduction period being sufficiently long. The latter point is consistent with observations from the recent literature on the duration of policy interventions¹⁶. In fact, the disease is quickly eradicated in the first scenario after the first wave, with 5.2% of cumulative infections and even a decrease in the socio-economic cost compared to the indefinite but mild policy discussed above, while the second (more severe, but shorter) choice of interventions yields a second wave with a final prevalence of 9.6% and a socio-economic cost that is almost doubled.

Finally, in Fig. 5d, we repeat the scenario observed in Fig. 5b but remove the factor of social influence. We find that the presence of social influence during the initial severe intervention period ensures a collective population response with a 99% adoption rate of self-protective behaviours (Fig. 5b); in contrast, the adoption rate is reduced to $\approx 60\%$ without social influence (Fig. 5d). However, during the phased reduction period, social influence accelerates a collective rejection of self-protective behaviours; in Fig. 5b, individuals overwhelmingly reject self-protective behaviour completely two weeks before the end of the phased reduction period (Supplementary Fig. S3). This resembles the difficulties experienced by some countries in controlling the exit out of a lockdown in the current COVID-19 pandemic³⁰. The crucial role played by social pressures as concluded from our simulation results and the resonance thereof in the COVID-19 reality indicate the need for epidemics models to include time-varying behavioural responses. The model predictions highlight

the challenges policy makers experience in designing interventions, but also provide important directions. For example, our model results indicate that it is more effective to focus on managing the duration and relaxation of the interventions, and our findings support the suggestion in⁵ of a closer examination of how to exploit social influence to marshal effective long-term responses to an epidemic. This analysis highlights the potential of our modelling paradigm in helping policy makers assess control actions to effectively address epidemic outbreaks. Its input parameters are closely related to observable properties of the epidemic as well as the population; the wealth of behavioural data currently being gathered in the context of the COVID-19 pandemic will therefore allow further refining of the model.

4 Conclusion

Inspired by evidence of the key role played by individuals' behavioural responses in shaping an epidemic outbreak, we have combined proven models of epidemics with an evolutionary game-based description of individual decision-making into a novel unified modelling paradigm. To our knowledge, this is the first time an epidemic model has addressed the complex decision-making process of a population responding to an epidemic. Different from existing behavioural models based on reactive responses¹⁻⁴ and from game theoretical models based on imitation^{31,32}, our paradigm models how individual decisions are influenced by a large range of time-varying factors, including government interventions, risk perceptions, irrationality and social interactions throughout the duration of an epidemic outbreak, from the outbreak to eradication. When applied to case studies of the spreading of gonorrhoea, the 1918-19 Spanish flu and COVID-19, the model

captures a wide range of realistic outcome scenarios and specifically reveals the impact of social influence and phasing out of government interventions on the persistence of an epidemic. As the framework is parsimonious and universal, with parameters rooted to the specifics of both population and epidemic, it enables well-founded predictions of the effectiveness of non-pharmaceutical policy interventions in terms of health costs and socio-economic costs.

Methods

Details of the network structure The two-layered network structure with a static influence layer and a time-varying physical contact layer is motivated by the observation that social relationships (e.g. between family members, friends, colleagues) typically change at a much slower pace than that of epidemic processes and thus can be assumed constant, while the network of physical contacts evolves at a time-scale comparable with the spread of the disease³³.

The contact layer is modelled using an activity-driven network (ADN)²². ADNs have emerged as a powerful paradigm to study the dynamical co-evolution of (i) the network structure, and (ii) the process unfolding at each node. ADNs have found successful application in mathematical epidemiology³⁴. The network formation process acts as follows. At each discrete time instant t , with probability a_i , individual i activates and generates a fixed number of contacts $m \geq 1$ with other individuals chosen uniformly at random in the population. These contacts are added to the link set $\mathcal{E}_C(t)$, contribute to the epidemic process, and are then removed before the next discrete time instant and the next activation of individuals. Despite their simplicity, which enables rigorous analytical treatment and fast numerical simulations^{22,35}, ADNs can capture important features of complexity that characterise real-world networks and are amenable to analytically-tractable extensions to include further features. Importantly, the proposed modelling paradigm can also use other time-varying network models, e.g. temporal switching networks³⁶.

Details of the SIS model According to the SIS mechanism described in the main paper, the contagion probability for a generic individual $i \in \mathcal{V}$ is

$$\mathbb{P}[x_i(t+1) = I | x_i(t) = S] = (1 - y_i(t)) (1 - (1 - \lambda)^{N_i(t)}) , \quad (5)$$

where

$$N_i(t) = |\{j \in \mathcal{V} : (i, j) \in \mathcal{E}_C(t), x_j(t) = I\}| \quad (6)$$

is the number of infectious individuals that have a link with node i at time t on the contact layer. While Eq. (5) posits that adoption of self-protective behaviour, viz. $y_i(t) = 1$, always makes the contagion probability equal to 0, the model can be generalised by introducing a parameter to reflect that self-protective behaviours have a probability in failing to prevent infection. The recovery process described in the main paper is governed by the following probabilistic rule:

$$\mathbb{P}[x_i(t+1) = S | x_i(t) = I] = \mu . \quad (7)$$

Details of the SEIR model In the SEIR model, individuals may have four different health states: they can be susceptible to the disease (S); exposed (E), i.e. already infected but asymptomatic; infected and symptomatic (I); or removed (R), accounting for both recoveries and deaths. The disease spreads as follows. At each discrete time-step t , every individual i that is susceptible (i.e. $x_i(t) = S$) and does not adopt self-protective behaviours (i.e. $y_i(t) = 0$) may become infected. Similar to the SIS model, we introduce a constant parameter $\lambda \in [0, 1]$, termed *infection probability*, which captures the probability that the infectious disease is transmitted from an infectious individual to a susceptible one through a link in the contact layer. After contagion, individuals become exposed (E). The disease propagates through contacts, each one independent of the others,

yielding

$$\mathbb{P}[x_i(t+1) = E | x_i(t) = S] = (1 - y_i(t)) (1 - (1 - \lambda)^{N_i(t)}), \quad (8)$$

where $N_i(t)$ is the number of neighbours of node i on the contact layer that are infectious at time t . Depending on the specifics of the disease, exposed (i.e. pre-symptomatic) individuals may be infectious or not, giving

$$N_i(t) = \begin{cases} |\{j \in \mathcal{V} : (i, j) \in \mathcal{E}_C(t), x_j(t) \in \{E, I\}\}| & \text{if exposed individuals are infectious,} \\ |\{j \in \mathcal{V} : (i, j) \in \mathcal{E}_C(t), x_j(t) = I\}| & \text{otherwise.} \end{cases} \quad (9)$$

Beside the contagion, two other mechanisms govern the epidemic process: the emergence of symptoms and the recovery process. Specifically, at each time-step t , every individual i that is exposed (E) has probability $\nu \in (0, 1]$ to become symptomatic, independent of the others, giving

$$\mathbb{P}[x_i(t+1) = I | x_i(t) = E] = \nu. \quad (10)$$

Then, infected individuals have probability $\mu \in (0, 1]$ to recover, independent of the others, giving

$$\mathbb{P}[x_i(t+1) = R | x_i(t) = I] = \mu. \quad (11)$$

Different from the SIS model, once removed, individuals are immunised and cannot be infected again.

Details of the decision-making mechanism Here, we provide with some additional details and comments on the decision-making mechanism. The parameter $\beta \in [0, \infty)$ and the log-linear learning dynamics in Eq. (16) model bounded rationality in an individual's decision-making process.

We have assumed for simplicity that β is homogeneous among all individuals in this work, but this is easily generalisable to be heterogeneous. Notice that if $\beta = 0$, individuals make decisions uniformly at random, while for $\beta \rightarrow \infty$, individuals apply perfect rationality to select the behaviour with highest payoff. This best-response behaviour is myopic, i.e. individuals do not look forward in time to optimise a sequence of decisions.

The risk perception function is a monotonic non-decreasing function of $z(t)$, capturing the fear of being infected that rises as the number of symptomatic individuals increase. In its simplest formulation (which will be adopted in the three case studies presented in this paper), it can be assumed to be a power function

$$r(z) = kz^\alpha, \quad (12)$$

with $k > 0$ and $\alpha > 0$. Specifically, $\alpha \in (0, 1)$ models cautious populations, where a small initial outbreak causes a large increase in the risk perception. The case $\alpha = 1$ captures a population whose reaction grows exactly proportionally to the epidemic prevalence observe. On the contrary, $\alpha > 1$ captures populations that underestimate the risk, and the epidemic prevalence must be large before the risk perception plays an important role in the decision-making process. The constant k is a scaling constant. In the main paper, we consider three different functions as archetypes of three different scenarios: a cautious population ($\alpha < 1/2$), a population with reaction proportional to the epidemic prevalence ($\alpha = 1$), and a slow reacting population ($\alpha = 2$). In all three cases we set $k = 3$.

Note that, in the absence of the accumulation of socio-economic costs ($\gamma = 0$) and without

policy interventions $u(t) = 0$, the risk perception function determines a critical prevalence

$$z^* = \min\{z : r(z) > 1 + c\}, \quad (13)$$

such that, $z(t) > z^*$ implies $\pi_i(1) > \pi_i(0)$, for any individual i . In other words, if the detectable prevalence exceeds z^* , each individual will always favour the adoption of self-protective behaviours, regardless of the behaviour of other individuals and of the presence of policy interventions.

We remark that the risk perception (as well as the cost of self-protection) is endogenous to each individual, different from the policy intervention $u(t)$, which is exogenous and from the social influence, which is determined by the network structure.

Evaluating the socio-economic impact The *health cost* H is a functional that quantifies the costs related to the health state of individuals and may have different definitions, depending on the epidemic model used and on the focus of the study. In our case studies, we define the health cost for the SEIR model as the total number of infections, i.e. the cumulative prevalence. Specifically, fixed a period of observation $T \geq 0$ (the duration of the epidemic outbreak), we define

$$H(T) = \frac{1}{n} |\{i : x_i(T) = R\}|. \quad (14)$$

Note that in the SIS model, the health cost may be defined as the average epidemic prevalence over the period of observation.

We define the per capita *socio-economic cost* over a fixed period of observation $T \geq 0$ (the duration of the epidemic outbreak) as the average cumulative immediate costs incurred by an

individual in the population, that is,

$$C := \frac{1}{n} \sum_{t=0}^T \sum_{i=1}^n c y_i(t). \quad (15)$$

Derivation of the epidemic threshold for the SIS model In the absence of cumulative frustration and for a fully mixed influence layer, we observe that

$$\mathbb{P}[y_i(t+1) = 0] = \frac{\exp\{\beta\pi_i(0)\}}{\exp\{\beta\pi_i(0)\} + \exp\{\beta\pi_i(1)\}} \quad (16)$$

has the same expression for all the nodes. In fact, if we define $\bar{y}(z)$ as the probability that a generic node adopts self-protective behaviours when the epidemic prevalence is equal to z , then, according to the strong law of large numbers, $\pi_i(0) = 1 - \bar{y}(z) - u(t) = 1 - \bar{y}(z) - \bar{u}$ (since the control is assumed to be a constant function) and $\pi_i(1) = \bar{y}(z) + r(z) - c$, which are independent of i . In a mean-field approach²⁴, we define $\theta(t) = \frac{1}{n} \sum_{i:x_i(t)=I} a_i$ as the average activity of infected nodes and $z_i(t) = \mathbb{P}[x_i(t) = I]$. Due to the strong law of large numbers, in the limit of large-scale systems $n \rightarrow \infty$, $z(t) = \frac{1}{n} \sum_{i=1}^n z_i(t)$ and $\theta(t) = \frac{1}{n} \sum_{i=1}^n a_i z_i(t)$. Hence, from the mean-field evolution of $z_i(t)$, given by

$$z_i(t+1) = z_i(t) - \mu z_i(t) + (1 - z_i(t))(1 - \bar{y}(z(t)))a_i z(t) + (1 - z(t))(1 - \bar{y}(z(t)))\lambda\theta(t), \quad (17)$$

we determine the following system of difference equations for the epidemic prevalence and the average activity of infected individuals, linearised about the disease-free equilibrium ($z = 0, \theta = 0$):

$$\begin{aligned} z(t+1) &= z(t) - \mu z(t) + m\lambda\langle a \rangle z(t)(1 - \bar{y}(0)) + m\lambda(1 - \bar{y}(0))\theta(t) \\ \theta(t+1) &= \theta(t) - \mu\theta(t) + m\lambda\langle a^2 \rangle z(t)(1 - \bar{y}(0)) + m\lambda\langle a \rangle(1 - \bar{y}(0))\theta(t). \end{aligned} \quad (18)$$

From standard theory on the stability of discrete-time linear time-invariant systems³⁷, the origin is stable if

$$\frac{\lambda}{\mu} < \frac{1}{m(\langle a \rangle + \sqrt{\langle a^2 \rangle})(1 - \bar{y}(0))}. \quad (19)$$

In fully-mixed influence layers, the probability for an individual to adopt self-protective behaviours $\bar{y}(z)$ can be derived by substituting $\pi_i(0) = 1 - \bar{y}(z) - \bar{u}$ and $\pi_i(1) = \bar{y}(z) + r(z) - c$ into Eq. (16), obtaining the equilibrium equation:

$$\bar{y} = \frac{e^{\beta(\bar{y}-c+r(z))}}{e^{\beta(\bar{y}-c+r(z))} + e^{\beta(1-\bar{y}-\bar{u})}}. \quad (20)$$

Even though it is not possible to derive a closed-form solution, we observe that at the inception of the epidemic outbreak, $y_i(0) = 0$ for all individuals and, for sufficiently small values of \bar{u} (i.e. $\bar{u}5.21 + c$), in the early stages it is verified that $\pi_i(0) > \pi_i(1)$. Hence, if the rationality β is sufficiently large, the equilibrium \bar{y} is close to 0 and can be approximated by Taylor-expanding the right-hand side of the equation, obtaining

$$\bar{y}(z) \approx \frac{e^{\beta(-c+r(z))}}{e^{\beta(1-\bar{u})} + (1 - \beta)e^{\beta(-c+r(z))}}. \quad (21)$$

Network parameters of the simulations In all the simulations, we consider $n = 10,000$ individuals (10 of them initially infected) connected on the influence layer through a Watts–Strogatz small-world network, which captures many features of real-world influence networks, including a clustered structure and the presence of long-range interactions³⁸. We set an average degree 8 and rewiring probability $1/8$, so that each node has on average 1 long-range interaction.

The contact layer is generated following an ADN with power-law distributed activities a_i

with exponent 2.09, as in Aiello et al.³⁹, and lower cutoff at $a_{\min} = 0.1$. We set $m = 1$ interactions per active node for gonorrhoea and $m = 13$ for Spanish flu and COVID-19, based on⁴⁰.

Epidemic parameters of the simulations In the three case studies we use two different classical epidemic models: the SIS and the SEIR model. The former is used for gonorrhoea, which is a sexually transmitted disease characterised by negligible protective immunity after recovery and negligible latency period (individuals are infectious on average the day after contagion)^{25,41}. An SEIR model is used to capture latency periods after contagion and immunity after recovery, which have been observed for the Spanish flu²⁶ and COVID-19⁸. In the two SEIR case studies we rely on slightly different implementations of the epidemic model. For Spanish flu, based on established evidence, we assume that exposed (pre-symptomatic) individuals are not infectious²⁶. For the COVID-19 case study, where the preliminary observations are fewer and there is no consensus on the infectiousness of asymptomatic individuals, we assume the worst-case scenario in which all exposed individuals are infectious.

The epidemic parameters are set from epidemiological data. Specifically, reliable estimations of the time from contagion to symptoms onset τ_E (for Spanish Flu and COVID-19) and the time from symptoms onset to recovery τ_I (for all three diseases) are available^{8,25,26}. Similar to⁸, from these data we define

$$\nu = 1 - \exp\left(-\frac{1}{\tau_E}\right), \quad \text{and} \quad \mu = 1 - \exp\left(-\frac{1}{\tau_I}\right). \quad (22)$$

Finally, the parameter λ is obtained from available estimations of the basic reproduction number R_0 for the three diseases^{8,25,26}. The basic reproduction number is defined as the average number

of secondary infections produced by an infected individual in a population where everyone is susceptible. Hence, if we define τ to be the average time that an individual is infectious ($\tau = \tau_I + \tau_E$ for COVID-19 and $\tau = \tau_E$ for Spanish flu), assuming independence between the time an individual is infectious and their activity, we compute

$$R_0 = \frac{1}{n} \sum_{i \in \mathcal{V}} (a_i + \langle a \rangle) m \lambda \tau = 2 \langle a \rangle m \lambda \tau, \quad (23)$$

which implies

$$\lambda = \frac{R_0}{2m \langle a \rangle \tau}. \quad (24)$$

The epidemic parameters computed using this procedure are the following.

- **Gonorrhoea.** We find $\lambda = 0.3626$ and $\mu = 0.1195$, where the time unit is a week.
- **Spanish Flu.** We obtain $\lambda = 0.066$, $\mu = 0.2164$ and $\nu = 0.4092$, where the time unit is a day.
- **COVID-19.** We compute $\lambda = 0.03$, $\mu = 0.1813$ and $\nu = 0.1813$, where the time unit is a day.

Decision-making parameters of the simulations We set a common level of rationality $\beta = 6$ in all simulations, which captures a moderate level of rationality so that individuals tend to maximise their payoff, but always have a small, non-negligible probability of adopting the behaviour with the lower payoff. Before detailing the parameters used in the three case studies, we provide a brief discussion on the relative order of magnitude between the model parameters, which guided our choices.

The decision-making process is based on the comparison between the two payoff functions in Eqs. (2a) and (2b). The contribution of social influence to the payoff is always bounded between 0 and 1. Hence, social influence is significant if the other terms do not have a higher order of magnitude. Consequently, policy interventions $u(t) > 1$ can be considered severe, since their effect is predominant with respect to social influence, while policies with $u(t) < 1$ are milder. The cost of self-protective behaviours consists of two terms: the immediate cost per unit-time c and the accumulation factor γ . Small values of c become negligible in the decision making process, while, to avoid the immediate cost dominating the other terms, we should assume $c < 1$. The accumulation factor γ captures the cost for continued periods in which an individual adopts self-protective behaviours. To model a non-negligible effect of the accumulation of socio-economic costs, we should guarantee that over long periods in which an individual consistently adopts self-protective behaviours, the frustration function saturates to a value comparable to the other terms. This can be achieved by imposing that

$$\lim_{t \rightarrow \infty} c + \sum_{s=1}^t \gamma^s c = \frac{c}{1 - \gamma} \approx 1, \quad (25)$$

yielding $c + \gamma \approx 1$ (note, the above equality was obtained using the geometric series). Specifically, values of $\gamma > 1 - c$ guarantees that self-protective behaviours are eventually dismissed, after the complete eradication of the disease or the policy intervention is switched off. We use the risk perception function $r(t) = kz^\alpha$ proposed in Eq. (12) with $\alpha = 1/2$ for cautious populations, $\alpha = 1$ to model proportional reactions, and $\alpha = 2$ for slow reacting populations. As observed in Eq. (13), the risk perception function determines a critical epidemic prevalence that triggers the adoption of self-protective behaviours even in the absence of interventions (in the presence of accumulation,

the immediate cost c in Eq. (13) is substituted by its saturation value from Eq. (25) $c/(1 - \gamma)$. We observe from Eq. (13) that risk perception becomes non-negligible if $k > 1 + \frac{c}{1-\gamma}$. To keep consistency throughout our simulations, we set $k = 3$, which is a value that verifies the condition above for all the choices of parameters c and γ we make in the simulations.

The decision-making parameters used for the three case studies are detailed in the following.

- Gonorrhoea.** We assume that the accumulation is negligible for gonorrhoea (where the use of protections has an immediate cost that typically does not accumulate, such as protective sexual barriers). Hence, for all three simulations, we fix the immediate cost to $c = 0.3$ and the accumulation factor $\gamma = 0$. No policy intervention is set, with $u(t) = 0$ for all $t \geq 0$. In the three simulations, we test three different risk perception function. Specifically, we consider a cautious population with $r(z) = 3\sqrt{z}$ in Fig. 3a, a population with a proportional reaction, $r(z) = 3z$ in Fig. 3b, and a population slow to react with $r(z) = 3z^2$ in Fig. 3c.
- Spanish flu.** Self-protective behaviours involve social distancing and closures of economic activities, which has been shown to typically yield an accumulation of psychological distress and economic losses^{18–20}. Hence, we assume a high accumulation factor $\gamma = 0.9$ and we fix $c = 0.1$, in light of our discussion above. To capture the slow reaction of the population due to the initial suppression of information (to keep morale during World War I)^{6,42}, we set $r(z) = 3z^2$. To further mirror real-world interventions by public authorities, we set an initial intervention level equal to $u(0) = 0$, which switches to $u(t) = \bar{u} = 0.5$ once 1% of the population is infected and then remains active for 28 days before being turned off again.

- COVID-19.** Similar as we did for the Spanish flu, we assume that accumulation is non-negligible by setting $\gamma = 0.75$. Note that we select a smaller value of γ than the one used for Spanish flu to capture how development in information and communications technologies has helped alleviate the negative impact of extended lockdown policies during COVID-19 outbreak. In view of the observations above, we fix $c = 0.3$. We consider a scenario in which individuals are slow to perceive COVID-19 as a real threat ($r(z) = 3z^2$), as happened in many countries including the UK and US⁴³. In Fig. 5a, we start with $u(0) = 0$, and then set the intervention as $u(t) = 0.7$ when 1% of the population is infected, which is then turned off if 14 consecutive days pass with $z(t) = 0$. In Fig. 5b and Fig. 5c, we consider scenarios involving an initial severe but constant lockdown policy followed by a phased reduction. In the first scenario (Fig. 5b), severe policies ($u(t) = 1.1$) are implemented for 28 days after reaching 1% of infections, after which $u(t)$ is linearly reduced to $u(t) = 0$ over 35 time-steps. In the second scenario (Fig. 5c), more severe policies ($u(t) = 1.25$) are implemented for the same period of 28 time-steps, after which $u(t)$ is linearly reduced to $u(t) = 0$ over a shorter time-window of 24 time-steps. Note that we select the intensity of policy interventions and the duration of the phased reduction to ensure that the cumulative intervention effort, $\sum_t u(t)$, over the policy intervention period, is equal in the two scenarios. Finally, in Fig. 5d, we tested the intervention scenario in Fig. 5b but in the absence of social influence. Specifically, we removed the first term in each the two payoff functions in Eqs. (2a) and (2b).

Data Availability All data generated or analysed during this study are included in this Article (and its Supplementary Information files).

Code Availability The code used in the simulations is available at <https://github.com/lzino90/behavior>.

References

1. Funk, S., Salathé, M. & Jansen, V. A. Modelling the influence of human behaviour on the spread of infectious diseases: a review. *J. R. Soc. Interface* **7**, 1247–1256 (2010).
2. Perra, N., Balcan, D., Goncalves, B. & Vespignani, A. Towards a Characterization of Behavior-Disease Models. *PLOS One* **6** (2011). URL <https://doi.org/10.1371/journal.pone.0023084>.
3. Wang, Z., Andrews, M. A., Wu, Z.-X., Wang, L. & Bauch, C. T. Coupled diseasebehavior dynamics on complex networks: A review. *Phys. Life Rev.* **15**, 1 – 29 (2015).
4. Verelst, F., Willem, L. & Beutels, P. Behavioural change models for infectious disease transmission: a systematic review (2010-2015). *J. R. Soc. Interface* **13**, 20160820 (2016).
5. Van Bavel, J. J. *et al.* Using social and behavioural science to support COVID-19 pandemic response. *Nat. Hum. Behav.* **4**, 460–471 (2020).
6. Markel, H. *et al.* Nonpharmaceutical Interventions Implemented by US Cities During the 1918-1919 Influenza Pandemic. *JAMA* **298**, 644–654 (2007).

7. Flaxman, S. *et al.* Estimating the effects of non-pharmaceutical interventions on COVID-19 in Europe. *Nature* (2020). URL <https://doi.org/10.1038/s41586-020-2405-7>.
8. Prem, K. *et al.* The effect of control strategies to reduce social mixing on outcomes of the COVID-19 epidemic in Wuhan, China: a modelling study. *Lancet Public Health* **5**, e261–e270 (2020).
9. Blume, L. The Statistical Mechanics of Best-Response Strategy Revision. *Games Econ. Behav.* **11**, 111–145 (1995).
10. Pastor-Satorras, R., Castellano, C., Van Mieghem, P. & Vespignani, A. Epidemic processes in complex networks. *Rev. Mod. Phys.* **87**, 925–979 (2015).
11. Giordano, G. *et al.* Modelling the COVID-19 epidemic and implementation of population-wide interventions in Italy. *Nat. Med.* **26**, 855–860 (2020).
12. Chinazzi, M. *et al.* The effect of travel restrictions on the spread of the 2019 novel coronavirus (COVID-19) outbreak. *Science* **368**, 395–400 (2020).
13. Vespignani, A. *et al.* Modelling COVID-19. *Nat. Rev. Phys.* **2**, 279–281 (2020).
14. Funk, S., Gilad, E., Watkins, C. & Jansen, V. A. A. The spread of awareness and its impact on epidemic outbreaks. *Proc. Natl. Acad. Sci. USA* **106**, 6872–6877 (2009).
15. Granell, C., Gómez, S. & Arenas, A. Dynamical interplay between awareness and epidemic spreading in multiplex networks. *Phys. Rev. Lett.* **111**, 128701 (2013).

16. López, L. & Rodó, X. The end of social confinement and COVID-19 re-emergence risk. *Nat. Hum. Behav.* **4**, 746–755 (2020).
17. Simon, H. A. Bounded rationality in social science: Today and tomorrow. *Mind Soc.* **1**, 25–39 (2000).
18. Nicola, M. *et al.* The socio-economic implications of the coronavirus pandemic (COVID-19): A review. *Int. J. Surg.* **78**, 185–193 (2020).
19. Qiu, J. *et al.* A nationwide survey of psychological distress among Chinese people in the COVID-19 epidemic: implications and policy recommendations. *Gen. Psychiatr.* **33**, e100213–e100213 (2020). URL <https://gpsych.bmj.com/content/33/2/e100213>.
20. Bartik, A. W. *et al.* The impact of covid-19 on small business outcomes and expectations. *Proc. Natl. Acad. Sci. USA* **117**, 17656–17666 (2020).
21. Brauer, F. & Castillo-Chavez, C. *Mathematical models in population biology and epidemiology* (Springer, New York NY, USA, 2012), 2nd edn.
22. Perra, N., Gonçalves, B., Pastor-Satorras, R. & Vespignani, A. Activity driven modeling of time varying networks. *Sci. Rep.* **2** (2012). URL <https://doi.org/10.1038/srep00469>.
23. Jackson, M. O. & Zenou, Y. Games on Networks. In *Handbook of Game Theory with Economic Applications*, vol. 4, chap. 3, 95–163 (Elsevier, 2015).

24. Mieghem, P. V., Omic, J. & Kooij, R. Virus spread in networks. *IEEE/ACM Trans. Netw.* **17**, 1–14 (2009).
25. Yorke, J. A., Hethcote, H. W. & Nold, A. Dynamics and Control of the Transmission of Gonorrhea. *Sex. Transm. Dis.* **5**, 51–55 (1978).
26. Mills, C. E., Robins, J. M. & Lipsitch, M. Transmissibility of 1918 pandemic influenza. *Nature* **432**, 904–906 (2004).
27. Barry, J. M. Pandemics: avoiding the mistakes of 1918. *Nature* **459**, 324–325 (2009).
28. Hatchett, R. J., Mecher, C. E. & Lipsitch, M. Public health interventions and epidemic intensity during the 1918 influenza pandemic. *Proc. Natl. Acad. Sci. USA* **104**, 7582–7587 (2007).
29. Washington Post. ‘If I get corona, I get corona’: Miami spring breakers say covid-19 hasn’t stopped them from partying. <https://www.washingtonpost.com/nation/2020/03/19/coronavirus-spring-break-party/>. Accessed: 2020/07/30.
30. The Guardian. Major incident declared as people flock to England’s south coast. <https://www.theguardian.com/world/2020/jun/25/major-incident-declared-as-people-flock-to-england-south-coast>. Accessed: 2020/07/24.
31. Poletti, P., Caprile, B., Ajelli, M., Pugliese, A. & Merler, S. Spontaneous behavioural changes in response to epidemics. *J. Theor. Biol.* **260**, 31–40 (2009).

32. Reluga, T. C. Game Theory of Social Distancing in Response to an Epidemic. *PLOS Comput. Biol.* **6** (2010). URL <https://doi.org/10.1371/journal.pcbi.1000793>.
33. Holme, P. & Saramäki, J. Temporal networks. *Phys. Rep.* **519**, 97–125 (2012).
34. Rizzo, A., Pedalino, B. & Porfiri, M. A network model for Ebola spreading. *J. Theor. Biol.* **394**, 212–222 (2016).
35. Zino, L., Rizzo, A. & Porfiri, M. Continuous-time discrete-distribution theory for activity-driven networks. *Phys. Rev. Lett.* **117**, 228302 (2016).
36. Valdano, E., Ferreri, L., Poletto, C. & Colizza, V. Analytical computation of the epidemic threshold on temporal networks. *Phys. Rev. X* **5**, 021005 (2015).
37. Rugh, W. *Linear System Theory*, vol. 2 (Prentice Hall, Upper Saddle River, NJ, 1996).
38. Watts, D. J. & Strogatz, S. H. Collective dynamics of ‘small-world’ networks. *Nature* **393**, 440–442 (1998).
39. Aiello, W., Chung, F. & Lu, L. A random graph model for power law graphs. *Exp. Math.* **10**, 53–66 (2001).
40. Mossong, J. *et al.* Social Contacts and Mixing Patterns Relevant to the Spread of Infectious Diseases. *PLOS Med.* **5** (2008). URL <https://doi.org/10.1371/journal.pmed.0050074>.
41. Lajmanovich, A. & Yorke, J. A. A deterministic model for gonorrhea in a nonhomogeneous population. *Math. Biosci.* **28**, 221–236 (1976).

42. Bootsma, M. C. J. & Ferguson, N. M. The effect of public health measures on the 1918 influenza pandemic in U.S. cities. *Proc. Natl. Acad. Sci. USA* **104**, 7588–7593 (2007).
43. Geldsetzer, P. Knowledge and Perceptions of COVID-19 Among the General Public in the United States and the United Kingdom: A Cross-sectional Online Survey. *Ann. Intern. Med.* **173**, 157–160 (2020).

Acknowledgements The work by M.Y. is partially supported by Optus Business. The work by L.Z. and M.C. is partially supported by the European Research Council (ERC-CoG-771687) and the Netherlands Organization for Scientific Research (NWO-vidi-14134). The work by A.R. is partially supported by Compagnia di San Paolo and by the Italian Ministry of Foreign Affairs and International Cooperation (Grant “Mac2Mic”).

Author Contributions M.Y. and L.Z. contributed equally. They designed the research, performed the analytical and numerical studies and wrote a first draft of the manuscript. A.R. and M.C. contributed equally to the formulation of the research questions, the supervision of the research, the interpretation and analysis of the results and to reviewing the manuscript. All the authors contributed to the present submission.

Competing Interests The authors declare that they have no competing interests.

Materials & Correspondence Correspondence and requests for materials should be addressed to Mengbin Ye. (email: mengbin.ye@curtin.edu.au)

SUPPLEMENTARY INFORMATION: Modelling epidemic dynamics under collective decision making

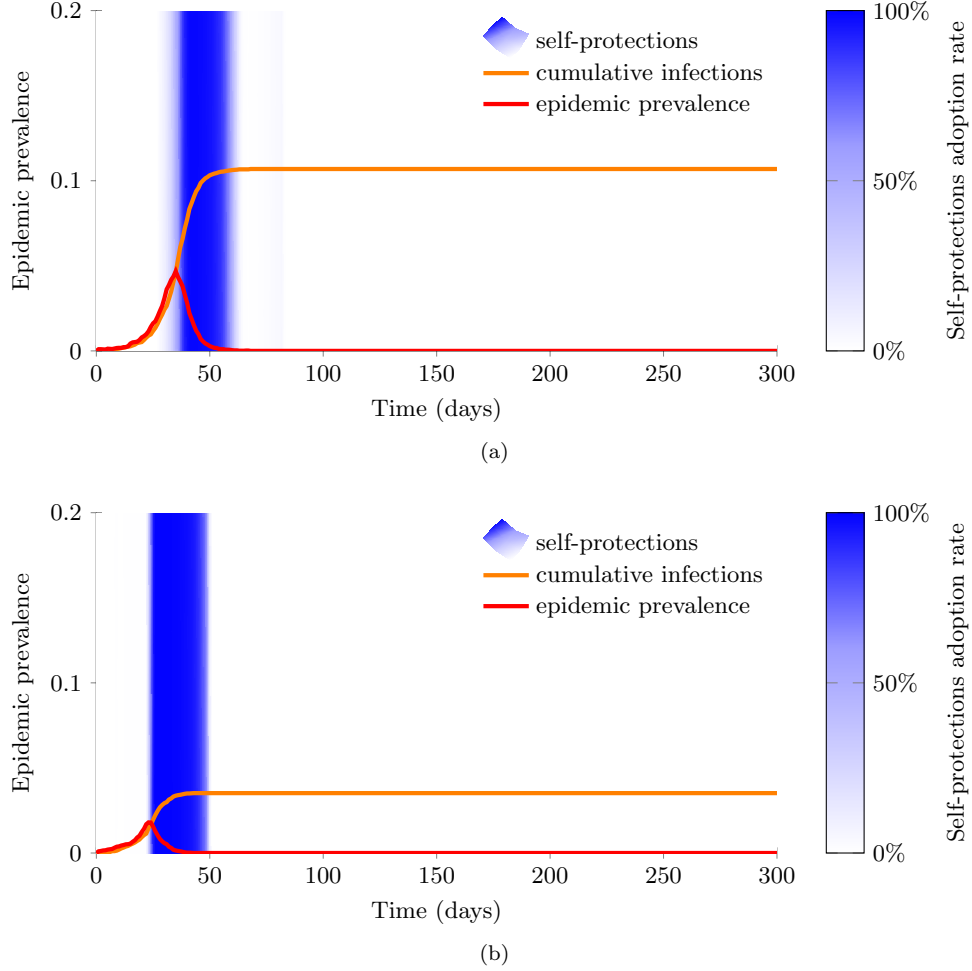


FIG. S1: **Extension of the Spanish Flu (SEIR) case study in the main article.** Prevalence of Spanish flu infections (red curve) and cumulative infections (orange curve) as a function of time as predicted by an SEIR model in combination with the co-evolution paradigm. The colour intensity of the blue vertical bands represents the fraction of adopters of self-protective behaviours. Consistent with the main article, we set $\gamma = 0.9$ and $c = 0.1$, and an initial intervention level equal to $u(0) = 0$, which switches to $u(t) = \bar{u} = 0.5$ once 1% of the population is infected and then remains active for \bar{T} days before being turned off again. In Fig. S1a, we set $r(z) = 3z^2$ (consistent with Fig. 4 in the main article), but double the intervention duration to $\bar{T} = 56$ days. In Fig. S1b, we retain the original $\bar{T} = 28$ days from Fig. 4 in the main article, but assume a more cautious population that is better informed, with $r(z) = 3\sqrt{z}$. In both figures, we see the epidemic outbreak is successfully halted after a single wave, either by a longer policy intervention or a population that has a heightened risk perception, in contrast to Fig. 4 of the main article. The impact of the outbreak is measured by health cost (a) $H = 10.69\%$ and (b) $H = 3.52\%$, and socio-economic cost (a) $C = 2.7$ and (b) $C = 2.5$, as detailed in the Methods.

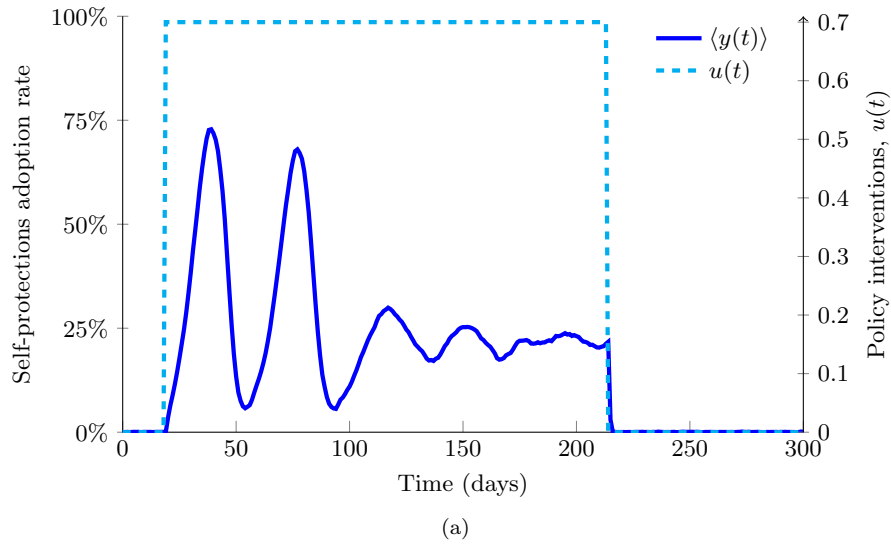


FIG. S2: Lag in the Adoption of Self-Protective Behaviours. This figure shows the same simulation as that in Fig. 5a of the main article. The adoption rate (blue solid curve) of self-protective behaviours, is quantified by $\langle y(t) \rangle = \frac{1}{n} \sum_{i=1}^n y_i(t)$, and the intervention policy (cyan dashed curve) shows an on/off constant policy intervention $u(t) = \bar{u} = 0.7$ being switched on when $z(t) > 0.01$, and switched off after no infections are reported for 14 consecutive days. Notice that although the intervention is introduced at $t = 19$, adoption of the self-protective behaviours peaks only 20 days later, at $t = 39$ with 73% adoption rate among the population^a. This allows us to conclude that the adoption of self-protective behaviours is delayed by social influence, which has an inertia effect, and the adoption rate improves because of individuals have an increasing perceived risk of infection as the epidemic grows. In contrast, all individuals revert back to standard behaviours at $t = 215$ days, almost immediately after the intervention policy ends at $t = 214$.

^a This adoption rate is well below the 99% seen in Fig. 5b and 5c of the main article, highlighting the necessity of severe interventions

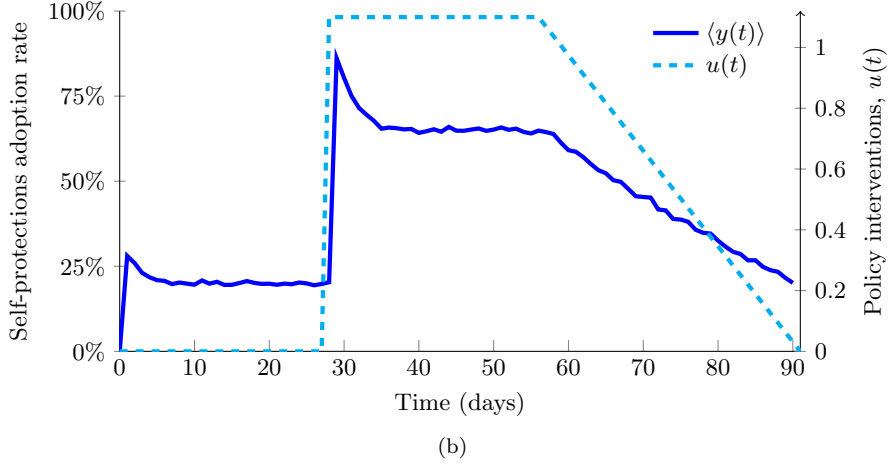
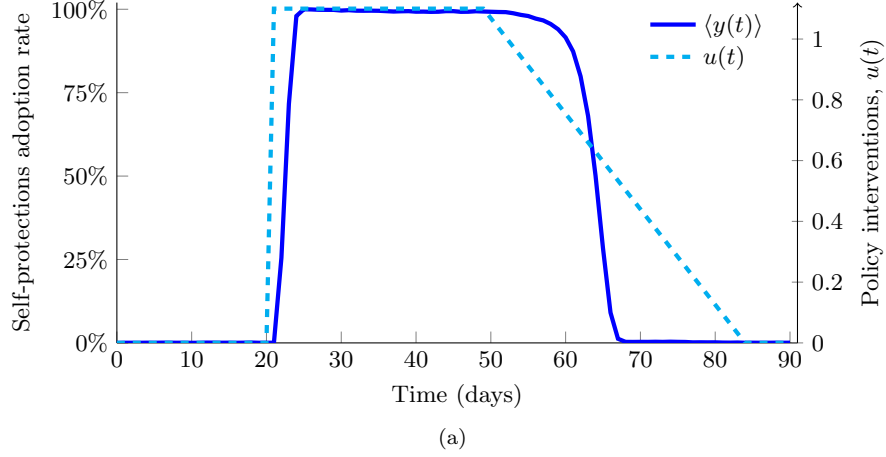


FIG. S3: The Role of Social Influence. Fig. S3a and Fig. S3b show the same simulation as that corresponding to Fig. 5b and 5d in the main article, respectively. The adoption rate (blue solid curve) of self-protective behaviours, is quantified by $\langle y(t) \rangle = \frac{1}{n} \sum_{i=1}^n y_i(t)$, and the intervention policy (cyan dashed curve) shows an initial severe and constant lockdown for 28 days after $z(t) > 0.01$, followed by a linear phased reduction over 35 days. Note that for the sake of clarity, the disease evolution is not shown here, and we only plot the time horizon up to the first policy intervention for Fig. 5d (in actuality, multiple interventions are necessary due to resurgent infection waves). Notice that in Fig. S3a, there is a delay of 3-4 days between the start of the intervention, and all individuals adopting self-protective behaviours, in contrast to Fig. S3b, where there is only a single day of delay. This supports the claim that social influence has an inertia effect in the beginning, but this delay is shortened by a severe intervention. During the 28 days of constant intervention, social influence acts to ensure a collective adoption of self-protective behaviours, countering the effects of accumulating costs $f_i(t)$, with $\langle y(t) \rangle \approx 0.99$ in Fig. S3a. In contrast, Fig. S3b sees an initial collective adoption driven by $u(t)$, but as costs accumulate, adoption drops to a constant of $\langle y(t) \rangle \approx 0.65$. However, once the phased reduction begins, we see the population with no social influence in Fig. S3b closely mirror the phased reduction. In contrast, social influence in Fig. S3a leads to a collective rejection of self-protective behaviours, with $\langle y(t) \rangle \approx 0$ by $t = 68$, over two weeks before the end of the phased reduction at $t = 84$ days.